SYNTHESIS AND CHARACTERIZATION OF
$Rb_x Mn[Fe(CN)]_6$ AND $Mn_3[Cr(CN)_6]_2$

PHUNG KIM PHU, NGUYEN MINH THUAN, TRAN NAM TRUNG
AND NGUYEN VAN MINH
Center for Nano Science and Technology, Hanoi National University of Education

Abstract. *We present the synthesis and detailed characterization of $Rb_x Mn[Fe(CN)_6]$ and $Mn_3[Cr(CN)_6]_2$ compounds. The composition of the materials significantly depends on the preparation conditions. Analysis of Raman spectroscopic results and X-ray powder diffraction data yielded a further assessment of the changes in structural features. The characteristic individual magnetic behavior, as well as the metal-to-metal charge-transfer capabilities of the various samples, could be related to significant changes within the structure that appear to be associated with the synthesis method used.*

I. INTRODUCTION

Recently, the development of photomagnetic molecular materials, in which magnetic properties can be controlled by light, has drawn increasing interest due to their potential relevance for high-density data storage and other technological applications. Several types of molecular materials with photomagnetic properties have been synthesized in the past few years. However, the researches on Prussian blue analogues have been focused mainly on properties of their bulk forms. In recent years, nano-sized Prussian blue analogues have emerged as a promising subject for applications to the nanomagnetic devices [1, 2]. These materials often exhibit novel size-dependent properties which show different properties from their bulk form [3]. There have been several techniques for preparing such materials. Here, we report a new approach for the growth of nanoparticles of cyano-bridged molecule-based magnets using an organic solvent, formamide and investigate structural, optical and magnetic properties of prepared products.

II. EXPERIMENTAL

The synthesis of $Rb_x Mn[Fe(CN)_6]$ and $Mn_3[Cr(CN)_6]_2$ samples has been carried out by a route similar to that described in Ref. [3] with some modifications. A starting mixture of RbCl (99.0%), $MnCl_2.4H_2O$ (99.0%), $K_3[Fe(CN)_6]$ and $K_3[Cr(CN)_6]$ (99,5%) was used as the precursor. The particle size of $Rb_x Mn_y[Fe(CN)_6]$ and $Mn_3[Cr(CN)_6]_2.nH_2O$ was found to be dependent on the ratio of formamide content to water content. Thus the particle size was controlled by varying the formamide-water ratio. In this report, two different types of samples are compared; the first type is made using water solvent only, hereafter called the water sample, and the second type is made using formamide solvent only, hereafter called the formamide sample.

Structural characterization was performed by means of X-ray diffraction using a D5005 diffractometer with CuK_α radiation. FE-SEM was operated by using a S4800 (Hitachi) microscope. The magnetic properties of the samples were investigated by a magnetic property measurement system PPMS 6000 (Quantum Design). Raman measurements were performed in a back scattering geometry using Jobin Yvon T 64000 triple spectrometer using 514.5 nm line of Ar ion laser.

III. RESULTS

From SEM images (figure 1) one can clearly see that the average sizes of $Rb_xMn[Fe(CN)_6]$ and $Mn_3[Cr(CN)_6]_2$ particles are uniform and about 200 nm. This indicated that the formamide solvent has prevented the particle growth.

The powder X-ray diffraction patterns of the samples are shown in Fig. 2. All of the diffraction peaks are readily indexed to a face centered cubic (FCC) phase [space group Fm3m (no.225)] with a lattice constant a = 10.67Å for $Rb_xMn[Fe(CN)_6]$ and 10.81Å for $Mn_3[Cr(CN)_6]_2$, and the other crystalline phases were not observed. The broadening of the X-ray diffraction peaks of the formamide samples is attributed to the lattice disorder and a dramatic reduction in the particle size (curves 2 and 2 in Fig. 2).

The compositions of the samples are confirmed by an energy-dispersive X-ray analysis (EDX), which reveals the presence of C, N, O, Fe, Mn, K, Cr and Rb. Figure 3 shows data for the formamide sample, which is almost the same as the data for the water sample. Moreover, there are small amounts of potassium impurities in the samples, because the potassium elements, which were introduced from the starting material $K3[Fe(CN)_6]$, were not completely washed out by water or ethanol. However, the EDX result proves that both of the samples are actually $Rb_xMn[Fe(CN)_6]$ and $Mn_3[Cr(CN)_6]_2$ Prussian blue, although their morphologies are quite different from each other.

Figure 4 shows the zero-field-cooled (ZFC) and field-cooled (FC) magnetization curves in the range of 250 K obtained for the $Rb_xMn[Fe(CN)_6]$ samples. Fig. 4a corresponds to the sample used water solvent, and Fig. 4b to the sample used formamide solvent, respectively. The FC and ZFC of sample used water solvent coincided (Fig. 4a), means that the magnetic property is similar to bulk sample. The ZFC curve of the sample used formamide shows a narrow peak at 7 K, which indicates the blocking temperature (TB) of the nanoparticles with a mean volume. As shown in Fig. 4b, there is a divergence between the field cooled (FC) and zero field cooled (ZFC) magnetization curves at 11 K, i.e., well below the Currie temperature, indicating that nanoparticles are single domain superparamagnets with a blocking temperature of 7 K, which corresponds to the maximum in the ZFC curve.

Figure 5 shows the magnetizations versus temperature plots of the prepared $Mn_3[Cr(CN)_6]_2.nH_2O$ nanomaterials. The nanoparticle showed a divergence between FC and ZFC magnetization curves below 42 K, and the ZFC magnetization curve showed maximum at 41 K. This temperature is lower than that of bulk form.

The magnetic susceptibility obeys the CurieWeiss law above 80 K. The determined Weiss constant is $\theta = -9$ K (not shown). The negative Weiss constant indicates antiferromagnetic exchange interactions between Mn and Cr ions. It is worthy to note that the
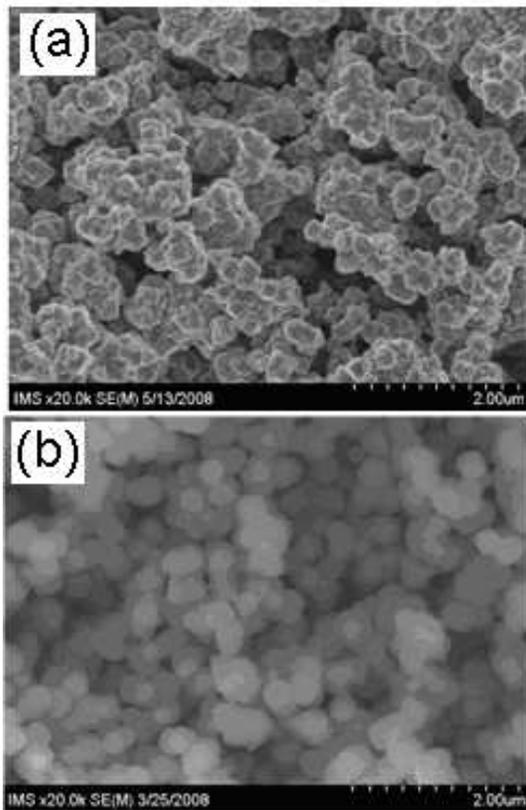
Fig. 1. SEM images of (a) $Rb_xMn[Fe(CN)_6]$ and (b) $Mn_3[Cr(CN)_6]_2$. For clarity, we show only image of sample prepared in formamide solution
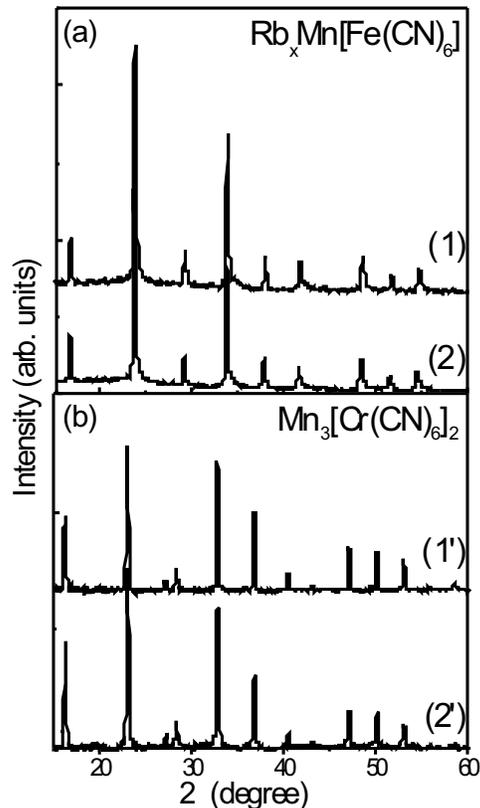
Fig. 2. XRD of (a): $Rb_xMn[Fe(CN)_6]$ and (b): $Mn_3[Cr(CN)_6]_2$ samples. (1), (1)label for H_2O and (2), (2) for formamide solution.

measured magnetic susceptibility and Weiss constant of Prussian blue particles are different from the common bulk. When the Prussian blue particle decreased to nanometer, the magnetic susceptibility and Weiss constant changed. It is mostly due to that the Prussian blue particle reaches the single domain limit. Therefore, the arrangement of Prussian blue particles has a significant effect on the magnetic properties of product.

The FC and ZFC of the "water" sample overlap each other (Fig. 4a), which means that the magnetic property is similar to that of the bulk sample. However, as shown in Fig. 4b for $Rb_xMn[Fe(CN)_6]$ and Fig. 5 for $Mn_3[Cr(CN)_6]_2$ there is a divergence between the field cooled (FC) and zero field cooled (ZFC) magnetization curves for the formamide sample, i.e., well below the Currie temperature, indicating that nanoparticles in the formamide sample are single domain superparamagnets with a blocking temperature. The FC curve increases with a decreasing temperature and never reaches saturation. This indicates that, even at the lowest temperature measured, a fraction of the particles is still in the superparamagnetic state. From a magneitc measurement of $Ni_3[Cr(CN)_6]_2$ nanocubes,
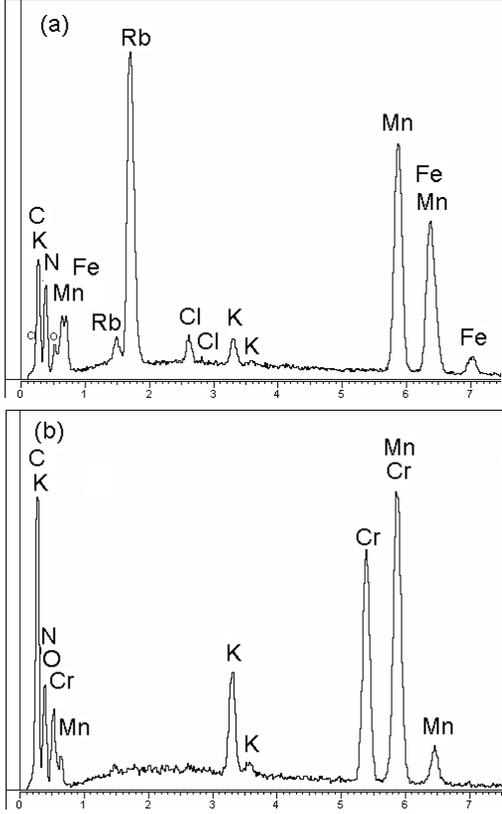
Fig. 3. EDX spectra of $Rb_xMn[Fe(CN)_6]$ and $Mn_3[Cr(CN)_6]_2$ Prussian blue. For clarity, we show spectra of only samples with formamide.
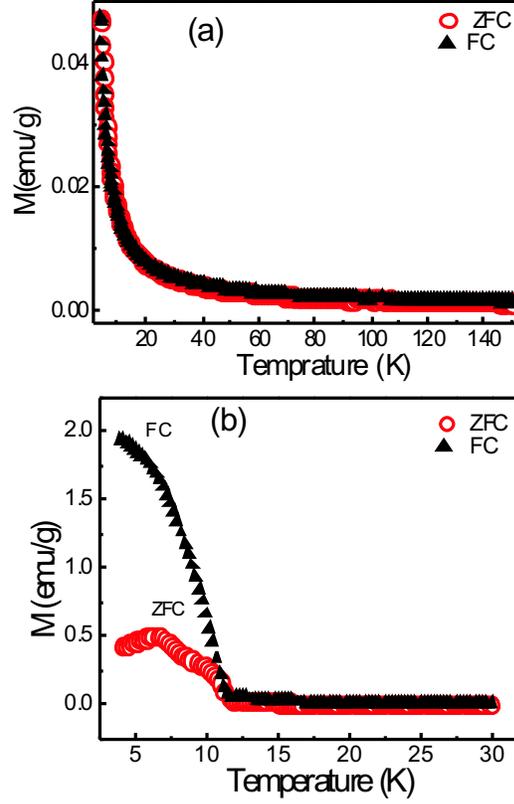
Fig. 4. FC and ZFC vs. temperature of the $Rb_xMn[Fe(CN)_6]$ samples used water (a) and formamide (b) solvent.

Mallah *et al.* [4] have confirmed that these nanoparticles behaved similarly to the bulk material at a high temperature. The increase in the FC values with decreasing temperatures and the maximum peak in the ZFC magnetization are indications of cluster spin-glass [5]. In a simple description specific to our samples, the cluster spin-glass state contains disordered interacting clusters, and each cluster consists of ferrimagnetically ordered Fe^{III}(LS, S = 1/2) and Mn^{II} (HS, S = 5/2) regions.

For PB analogs, the Curie temperature TC is expressed as in Ref. [6],

$$T_c = [2(Z_{ij}Z_{ji})^{1/2}|J_{ij}|/3k_B][S_i(S_i + 1)S_j(S_j + 1)]^{1/2}, \qquad (1)$$

where i=j=Fe^{III}, S_i=S_j=5/2, Z_{ij} or Z_{ji} is the number of the nearest-neighbor $i(j)$-site ions surrounding a $j(i)$-site ion, k_B is the Boltzmann constant, and J is the magnetic interaction constant. As the lattice parameter of nano-sized crystals does not change, we assume that the magnetic interaction constant J_{ij} between the Fe^{3+} ions of the PB nanoparticle in the "formamide sample is almost the same as that of the bulk sample. Therefore, the decrease in the Curie temperature T_C of the PB nanoparticle is perhaps
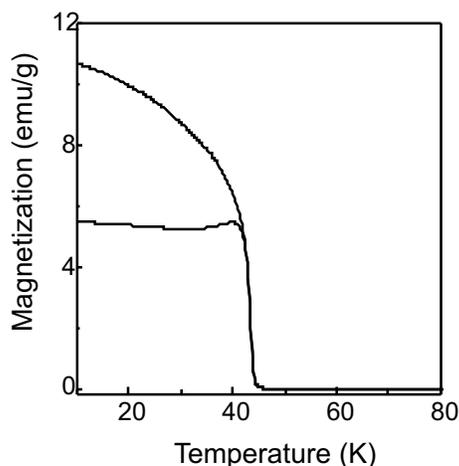
Fig. 5. Magnetization vs. temperature of $Mn_3[Cr(CN)_6]_2.nH_2O$ nanoparticle.
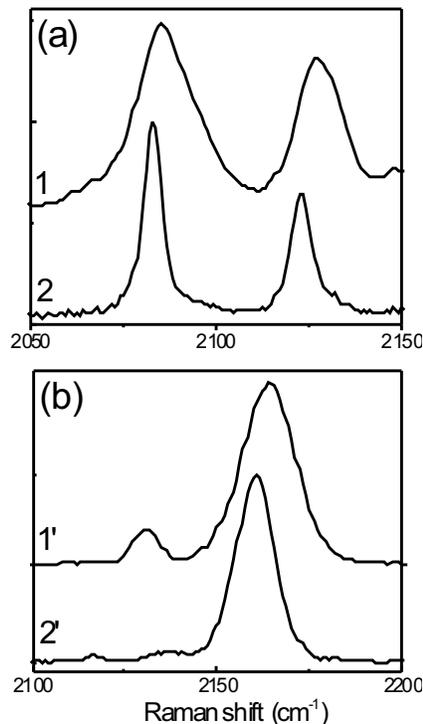
Fig. 6. Raman spectra of (a) $Rb_xMn[Fe(CN)_6]$ and (b) $Mn_3[Cr(CN)_6]_2.nH_2O$ nanoparticle.

due to the diminution of the average number of nearest magnetic interaction neighbors in the PB particle in comparison with the perfect crystal structure. Furthermore, defects could be present on the surface or inside of the Prussian blue particle, which may also affect the T_C.

The Raman spectra of both samples were shown in Fig. 6. The presence of water molecules, different sites for the Rb+ ions, defects such as missing $Fe(CN)_6$ units, etc., eventually lead to a lowering of the local symmetry. This is true for both the IR and Raman data. In contrast to IR absorption spectra, Raman spectra are not obscured by water lines, which give a cleaner access to specific molecular vibrations. Raman spectra of the studied compounds in the spectral region 2000-2300 cm^{-1} are dominated by two strong Raman bands that are centered in the vicinity of 2075 and 2175 cm^{-1}, and 2130 and 2170 cm^{-1} for $Rb_xMn[Fe(CN)_6]$ and $Mn_3[Cr(CN)_6]_2.nH_2O$, respectively (see Figure 6). In addition, a rather weak Raman band (∼5% of the total amplitude) is found around 2080 cm^{-1}. The measured Raman spectra can be interpreted in analogy with the IR absorption data, where the CN stretching mode corresponding to the band centered around 2175 cm^{-1} for $Rb_xMn[Fe(CN)_6]$ (and 2170 cm^{-1} $Mn_3[Cr(CN)_6]_2$) is attributed to CN ligands linking Fe^{III} (Cr^{III}) and Mn^{II} ions, whereas the broad band centered around 2075 cm^{-1} (2130 cm^{-1}) is assigned to CN ligands located between Fe^{II} (Cr^{III}) and Mn^{III} ions. Therefore, in

these samples, there exist both Mn^{II} and Mn^{III} as well as Cr^{II} and Cr^{III}. The broadening of the peak of sample using formamide related to size effect [7].

IV. CONCLUSIONS

In this work, we have developed a new approach for the growth $Rb_xMn[Fe(CN)_6]$ and $Mn_3[Cr(CN)_6]_2.nH_2O$ nanoparticle samples using formamide solvent. It is shown that the size has affected the structural, Raman scattering and magnetic property of samples. The ZFC curve of the nanoparticle sample shows a narrow peak, which indicates the blocking temperature (TB) of the nanoparticles with a mean volume. The increase in the FC values with decreasing temperatures and the maximum peak in the ZFC magnetization are indications of cluster spin-glass behavior.

ACKNOWLEDGEMENTS

REFERENCES

[1] P.H. Zhou, D.S. Xue, H.Q. Luo, X.G. Chen, *Nano Lett.* **2** (2002) 845.
[2] P.A. Berseth, J.J. Sokol, M.P. Shores, J.L. Heinrich, J.R. Long, *J. Am. Chem. Soc.* **122** (2000) 9655.
[3] V. Vien, N. V. Minh, H. I. Lee, J. M. Kim, Y. Kim, S. J. Kim, *Mater. Chem. and Phys.* **107** (2008) 6.
[4] T. Mallah, S. Thiebaut, M. Verdaguer and P. Veillet, *Science* **262** (1993) 1554.
[5] J.A. Mydosh, *Spin Glasses*, Taylor & Francis, Washington DC, 1993.
[6] S. Ohkoshi, T. Iyoda, A. Fujishima, and K. Hashimoto, *Phys. Rev.* **B56** (1997) 11642.
[7] M. Fox, *Optical Properties of Solids*, Oxford University Press, (2001) 115.

Received 07 July 2010.